Early-Onset, Slow Progression of Cone Photoreceptor Dysfunction and Degeneration in CNG Channel Subunit CNGB3 Deficiency

Jianhua Xu,[1] *Lynsie Morris,*[1] *Steven J. Fliesler,*[2,3,4] *David M. Sherry,*[1,5,6] *and Xi-Qin Ding*[1]

Purpose. To investigate the progression of cone dysfunction and degeneration in CNG channel subunit CNGB3 deficiency.

Methods. Retinal structure and function in CNGB3$^{-/-}$ and wild-type (WT) mice were evaluated by electroretinography (ERG), lectin cytochemistry, and correlative Western blot analysis of cone-specific proteins. Cone and rod terminal integrity was assessed by electron microscopy and synaptic protein immunohistochemical distribution.

Results. Cone ERG amplitudes (photopic b-wave) in CNGB3$^{-/-}$ mice were reduced to approximately 50% of WT levels by postnatal day 15, decreasing further to approximately 30% of WT levels by 1 month and to approximately 20% by 12 months of age. Rod ERG responses (scotopic a-wave) were not affected in CNGB3$^{-/-}$ mice. Average CNGB3$^{-/-}$ cone densities were approximately 80% of WT levels at 1 month and declined slowly thereafter to only approximately 50% of WT levels by 12 months. Expression levels of M-opsin, cone transducin α-subunit, and cone arrestin in CNGB3$^{-/-}$ mice were reduced by 50% to 60% by 1 month and declined to 35% to 45% of WT levels by 9 months. In addition, cone opsin mislocalized to the outer nuclear layer and the outer plexiform layer in the CNGB3$^{-/-}$ retina. Cone and rod synaptic marker expression and terminal ultrastructure were normal in the CNGB3$^{-/-}$ retina.

Conclusions. These findings are consistent with an early-onset, slow progression of cone functional defects and cone loss in CNGB3$^{-/-}$ mice, with the cone signaling deficits arising from disrupted phototransduction and cone loss rather than from synaptic defects. (*Invest Ophthalmol Vis Sci.* 2011;52:3557–3566) DOI:10.1167/iovs.10-6358

From the [1]Department of Cell Biology, University of Oklahoma Health Sciences Center, Oklahoma City, Oklahoma; [2]Research Service, Veterans Administration Western New York Healthcare System, Buffalo, New York; [3]Departments of Ophthalmology (Ira G. Ross Eye Institute/Vision Research Center) and Biochemistry, University at Buffalo/State University of New York, Buffalo, New York; [4]SUNY Eye Institute, Buffalo, New York; and [5]Oklahoma Center for Neurosciences and [6]Department of Pharmaceutical Sciences, University of Oklahoma Health Sciences Center, Oklahoma City, Oklahoma.

Supported by National Center for Cancer Resources Grant P20 RR017703 (XQD); National Institutes of Health/National Eye Institute Grants P30 EY12190 (DMS, XQD), R01 EY019490 (XQD), and R01 EY007361 (SJF); an unrestricted grant from Research to Prevent Blindness (SJF); and grants from the American Health Assistance Foundation (XQD) and the Oklahoma Center for the Advancement of Science and Technology (DMS, XQD).

Submitted for publication August 6, 2010; revised December 1, 2010; accepted December 20, 2010.

Disclosure: **J. Xu**, None; **L. Morris**, None; **S.J. Fliesler**, None; **D.M. Sherry**, None; **X.-Q. Ding**, None

Corresponding author: Xi-Qin Ding, 940 Stanton L. Young Boulevard, BMSB 553, Oklahoma City, OK 73104; xi-qin-ding@ouhsc.edu.

Photoreceptor cyclic nucleotide-gated (CNG) channels are localized to the plasma membrane of photoreceptor outer segments and play a pivotal role in phototransduction.[1,2] In the dark, cGMP binding activates rod CNG channels, allowing a steady cation current to flow into the outer segments. Light triggers a sequence of enzymatic reactions that leads to hydrolysis of cGMP, causing the channel to close. On channel closure, the inward current ceases and the cell hyperpolarizes, inhibiting synaptic transmission to second-order neurons. An analogous phototransduction scheme exists in cones, which are responsible for color vision and vision in bright illumination when rods are saturated. However, light sensitivity, cGMP sensitivity, Ca^{2+} permeation, and functional modulation differ profoundly between rod and cone CNG channels.[3–5] CNG channels are composed of two structurally related subunit types, the A and B subunits. The rod channel consists of CNGA1 and CNGB1 subunits, whereas the cone channel is composed of CNGA3 and CNGB3 subunits. Heterologous expression studies have shown that the A subunits are responsible for the ion-conducting activity of the channel, whereas the B subunits function as modulators.[2,6]

Mutations in the rod CNG channel were identified in patients with retinitis pigmentosa,[7] whereas mutations in the cone CNG channel have been associated with a variety of cone diseases, including achromatopsia, progressive cone dystrophy, and early-onset macular degeneration.[8–11] To date more than 70 mutations have been identified in genes encoding the human CNGA3 and CNGB3 subunits, with mutations in CNGB3 alone found in more than 50% of patients with achromatopsia,[9] a retinal disorder that affects approximately 1 in every 33,000 Americans. The condition is associated with color blindness, visual acuity loss, extreme light sensitivity, and nystagmus.[8,11,12] The most frequently occurring mutation in CNGB3 is the Thr383fsx mutation, which accounts for more than 80% of all CNGB3 mutant alleles.[9,13,14] This frame-shift mutation results in truncation of the pore-forming loop and the C-terminal cytoplasmic domain; as a result, no intact CNGB3 is formed. Thus, a loss-of-function defect is the primary mechanism of action for CNGB3 mutation in humans.

Although CNGB3 shares a common topology with CNGA3 and has a pore-forming region, this subunit, when expressed alone, does not form a functional channel, in contrast to CNGA3, which forms a functional homomeric channel.[6,15] Heteromeric CNGA3/CNGB3 channels display properties typical of native CNG channels,[6,16] suggesting that CNGB3 modulates the channel's physiological properties in vivo. Our previous experimental work showing the interaction between CNGA3 and CNGB3 in the mouse retina[17] and cone defects in CNGB3$^{-/-}$ mice[18] strongly supports this view. Here we investigate the progression of cone defects caused by CNGB3 deficiency. CNGB3$^{-/-}$ mice displayed an early-onset, slow progression of cone dysfunction and degeneration, similar to the human achromatopsia found in patients with mutations in

CNGB3. Furthermore, photoreceptor terminals appeared normal in the CNGB3$^{-/-}$ retina, suggesting that deficits in cone signaling result from disrupted phototransduction and cone loss rather than from synaptic defects. Thus, the CNGB3$^{-/-}$ mouse line will be a valuable model with which to study the functional and structural role of CNGB3 in cones and in retinal pathogenesis associated with achromatopsia.

Materials and Methods

Mice, Antibodies, and Other Materials

The CNGB3$^{-/-}$ mouse line (on a C57BL/6N background) was generated by targeted deletion (Deltagen Inc., San Mateo, CA), as described previously.[18] WT mice (C57BL/6) were purchased from Charles River Laboratories (Wilmington, MA). All mice were maintained under cyclic light (12-hour light/12-hour dark) conditions. Cage illumination was approximately 7 foot-candles during the light cycle. All experiments were approved by the local Institutional Animal Care and Use Committees (University of Oklahoma Health Sciences Center, Oklahoma City, OK) and conformed to the guidelines on the care and use of animals adopted by the Society for Neuroscience and the Association for Research in Vision and Ophthalmology (Rockville, MD).

Affinity-purified rabbit polyclonal antibodies against mouse M-opsin and cone arrestin (CAR) were provided by Cheryl Craft (University of Southern California, Keck School of Medicine). Rabbit polyclonal antibody against mouse S-opsin was provided by Muna Naash (University of Oklahoma Health Sciences Center). Rabbit polyclonal antibody against cone transducin α-subunit (Gnat2) was obtained from Santa Cruz Biotechnology, Inc. (Santa Cruz, CA). Monoclonal anti–actin antibody was purchased from Abcam, Inc. (Cambridge, MA). Mouse monoclonal antibody directed against C-terminal binding protein 2 (CtBP2) was purchased from BD Transduction Laboratories (San Jose, CA). Rabbit polyclonal anti–complexin 3 was from Synaptic Systems (Göttingen, Germany). Biotinylated peanut agglutinin (PNA) and streptavidin-FITC were purchased from Vector Laboratories (Burlingame, CA) and Sigma-Aldrich (St. Louis, MO), respectively. Wheat germ agglutinin (WGA) and PNA conjugated to AlexaFluor-488 or -568, and fluorescent goat anti–mouse and goat anti–rabbit secondary antibodies conjugated to AlexaFluor-488, -568, or -647, were from Invitrogen-Molecular Probes (Carlsbad, CA). Horseradish peroxidase (HRP)-conjugated anti–rabbit or anti–mouse secondary antibodies were purchased from Kirkegaard & Perry Laboratories Inc. (Gaithersburg, MD).

Recording of Electroretinograms

Full-field ERG testing was carried out as described previously.[19] Briefly, after overnight dark adaptation, animals were anesthetized by intraperitoneal injection of 85 mg/kg ketamine and 14 mg/kg xylazine. ERGs were recorded using an LKC Technologies (Gaithersburg, MD) system. Potentials were recorded using a platinum wire contacting the corneal surface through a layer of 2.5% methylcellulose. For assessment of scotopic responses, a stimulus intensity of 1.89 log cd · s/m^2 was presented to dark-adapted dilated mouse eyes in a Ganzfeld (GS-2000; Nicolet Instruments, Inc., Madison, WI). To evaluate photopic responses, mice were adapted to a 1.46 log cd · s/m^2 light for 5 minutes, and then a light intensity of 1.89 log cd · s/m^2 was given. Responses were differentially amplified, averaged, and stored using a signal averaging system (Compact-4; Nicolet Instruments, Inc.).

Eye Preparation, Immunohistochemistry, and Confocal Microscopy

Mouse retinal whole mounts or cross-sections were prepared for immunohistochemical analysis, as described previously.[19,20] For whole mount preparations, eyes were enucleated, marked at the superior pole with green dye, and fixed in 4% formaldehyde (Polysciences, Inc., Warrington, PA) for 5 to 10 minutes. The cornea and lens were removed, and the eyes were fixed in 4% formaldehyde at 4°C overnight. The retina was then marked for orientation with a small cut left of the superior portion, and the retina was isolated. For retinal sections, mouse eyes were enucleated and fixed in 4% formaldehyde in 0.1 M sodium phosphate buffer, pH 7.4, at 4°C overnight. The superior portion of the cornea was marked for orientation before enucleation. Fixed eyes were then stored in 70% ethanol until processed and embedded in paraffin. Paraffin sections (5-μm thickness) passing vertically through the retina were prepared using a Leica (Wetzlar, Germany) microtome.

Immunohistochemical labeling of cones using anti–opsin antibodies and PNA was performed as described previously.[17] Briefly, retinal whole mounts or sections were blocked in PBS containing 5% BSA and 0.5% Triton X-100 for 1 hour at room temperature. Primary antibody incubation (rabbit polyclonal anti–M-opsin, 1:500; rabbit polyclonal anti–S-opsin, 1:500) was performed at room temperature for 2 hours. After AlexaFluor-488 or -568 or FITC-conjugated secondary antibody incubation and rinses, slides were mounted and coverslipped. PNA immunohistochemistry was performed using biotinylated PNA (1:50) and streptavidin-FITC (1:200). Fluorescent signals were imaged using a fluorescence microscope (AX70; Olympus Corp., Center Valley, PA) with imaging software (QCapture; QImaging Corp., Surrey, BC, Canada) or a confocal laser scanning microscope (IX81-FV500; Olympus, Melville, NY) (using excitation wavelengths of 543 nm for AlexaFluor-568 and 488 nm for FITC) with imaging software (FluoView; Olympus, Melville, NY). Fluorescence labeling intensities of different regions of the retinal sections (outer segment [OS], outer nuclear layer [ONL], and outer plexiform layer [OPL]) were analyzed using the intensity mapping feature of the software as described previously.[21,22] Evaluation of cone density in retinal whole mounts was performed as described by Komeima et al.[23] Briefly, images were taken using a 40× objective on an Olympus microscope approximately 1 mm from the optic nerve in the center of each quadrant. Image scale was calibrated, and cones were counted in four regions, each with dimensions of 125 μm × 125 μm (1.56 × 10^4 μm^2; 500 × 500 pixels), using imaging software (Image Pro 6; Media Cybernetics, Inc., Bethesda, MD). Averages of the counts from four regions of the quadrants were analyzed and graphed using graphing and statistics software (Prism; GraphPad Software, San Diego, CA).

To assess the integrity of photoreceptor synaptic terminals, paraffin sections prepared from WT and CNGB3$^{-/-}$ mouse eyes were triple labeled using methods similar to those described previously.[24] Briefly, sections were deparaffinized and antigen was retrieved in citrate buffer and incubated in primary antibody overnight at 4°C. Mouse monoclonal antibody directed against CtBP2 (diluted 1:1000) was used to label synaptic ribbons. Rabbit polyclonal antibody against complexin 3 (diluted 1:1000) was used to selectively label cone terminals. Primary antibody was removed, and binding of primary antibodies was visualized using an appropriate combination of fluorescent goat anti–mouse and goat anti–rabbit secondary antibodies (diluted 1:200) and fluorescent conjugates of WGA or PNA (diluted 1:20–1:40) to visualize rod and cone terminal placement in the OPL and flat contacts onto cone terminals. After secondary antibody treatment, sections were rinsed and mounted using mounting medium plus DAPI (Prolong Gold; Invitrogen-Molecular Probes, Carlsbad, CA) to retard bleaching and visualize nuclei. Sections were imaged using an epifluorescence microscope (BX61-WI; Olympus America, Center Valley, PA), a camera (ORCA-ER; Hamamatsu, Bridgewater, NJ), and software (Slidebook; Intelligent Imaging Innovations, Denver, CO). Figures were prepared by calibrating image scale, exporting images to image editing software (Photoshop; Adobe, Mountain View, CA), and adjusting brightness, contrast, and threshold to highlight specific labeling.

Retinal Membrane Preparation, SDS-PAGE, and Western Blot Analysis

Protein SDS-PAGE and Western blot analysis were performed as described previously.[17] Briefly, retinas were homogenized in homogenization buffer (10 mM Tris-HCl, pH 7.4, 1 mM EDTA, 200 mM sucrose,

1 mM phenylmethylsulfonyl fluoride). Nuclei and cell debris were removed from the homogenate by centrifugation at 1000*g* for 10 minutes at 4°C. The resultant supernatant was centrifuged at 16,000*g* for 30 minutes at 4°C. Resultant membranes were used in Western blot analysis.

Retinal membrane proteins were subjected to SDS-PAGE and transferred onto polyvinylidene difluoride membranes. After 1 hour of blocking in 5% nonfat milk at room temperature, blots were incubated with primary antibody (anti–M-opsin, 1:2000; anti–Gnat2, 1:500; anti–CAR, 1:2000; or anti–actin, 1:5000) overnight at 4°C. After rinsing in Tris-buffered saline with 0.1% Tween 20, blots were incubated with HRP-conjugated secondary antibodies (at 1:5000 for anti–actin; 1:25,000 for other antibodies) for 1 hour at room temperature. Chemiluminescent substrate (SuperSignal West Dura Extended Duration; Pierce, Rockford, IL) was used to detect binding of the primary antibodies to their cognate antigens. Images were captured using a digital imaging system (Kodak Image Station 4000R; Carestream Molecular Imaging, New Haven, CT), and densitometric quantification was performed using Kodak molecular imaging software.

Transmission Electron Microscopy

Mouse eye samples were prepared for transmission electron microscopy, as described previously.[19,20] Briefly, mouse eyes were fixed in 4% formaldehyde in 0.1 M sodium phosphate buffer, pH 7.4, for 16 hours at 4°C and were transferred to PBS or 0.1 M sodium phosphate buffer, pH 7.4, containing 0.02% sodium azide, for storage until processing and embedding in plastic resin. Tissue sections were obtained with a microtome (Ultracut E; Reichert-Jung, Wetzlar, Germany) using a diamond knife. Thin sections (600–800 Å) were collected on copper 75/300 mesh grids for conventional EM analysis and stained with 2% (wt/vol) uranyl acetate and Reynolds' lead citrate. Sections were viewed with an electron microscope (100CX; JEOL, Tokyo, Japan) at an accelerating voltage of 60 keV, and images were captured at 5000× to 30,000× magnification.

Results

Early-Onset, Slow Progression of Cone Dysfunction in CNGB3$^{-/-}$ Mice

We evaluated cone function in CNGB3$^{-/-}$ mice at different ages (from postnatal [P] 15 days to 18 months) by full-field photopic ERG recordings. The b-waves of the photopic ERG responses were used to evaluate the light responses of cones.[19,25–28] Impaired photopic ERG response was already apparent by P15. At this age, the cone-driven response in WT mice was approximately 40% of the level detected in WT mice at 1 month, whereas the response in CNGB3$^{-/-}$ mice was approximately 50% of the age-matched WT level (Fig. 1A). The difference between CNGB3$^{-/-}$ and WT mice was further increased at 1 month, with the response in CNGB3$^{-/-}$ mice approximately 30% of the WT level. This residual cone response declined slowly afterward. Figure 1A shows photopic ERG b-wave amplitudes from CNGB3$^{-/-}$ mice at different ages. One-way ANOVA showed that the ERG response in CNGB3$^{-/-}$ mice at 3 months of age was not statistically different from that in CNGB3$^{-/-}$ at 1 month. However, a further progressive decrease in ERG b-wave amplitude was observed in CNGB3$^{-/-}$ mice after 6 months of age. Compared with the photopic b-wave amplitude of CNGB3$^{-/-}$ mice at 1 month, the b-wave amplitude was reduced by approximately 30%, 45%, and 55% at 12, 15, and 18 months, respectively. In contrast, no

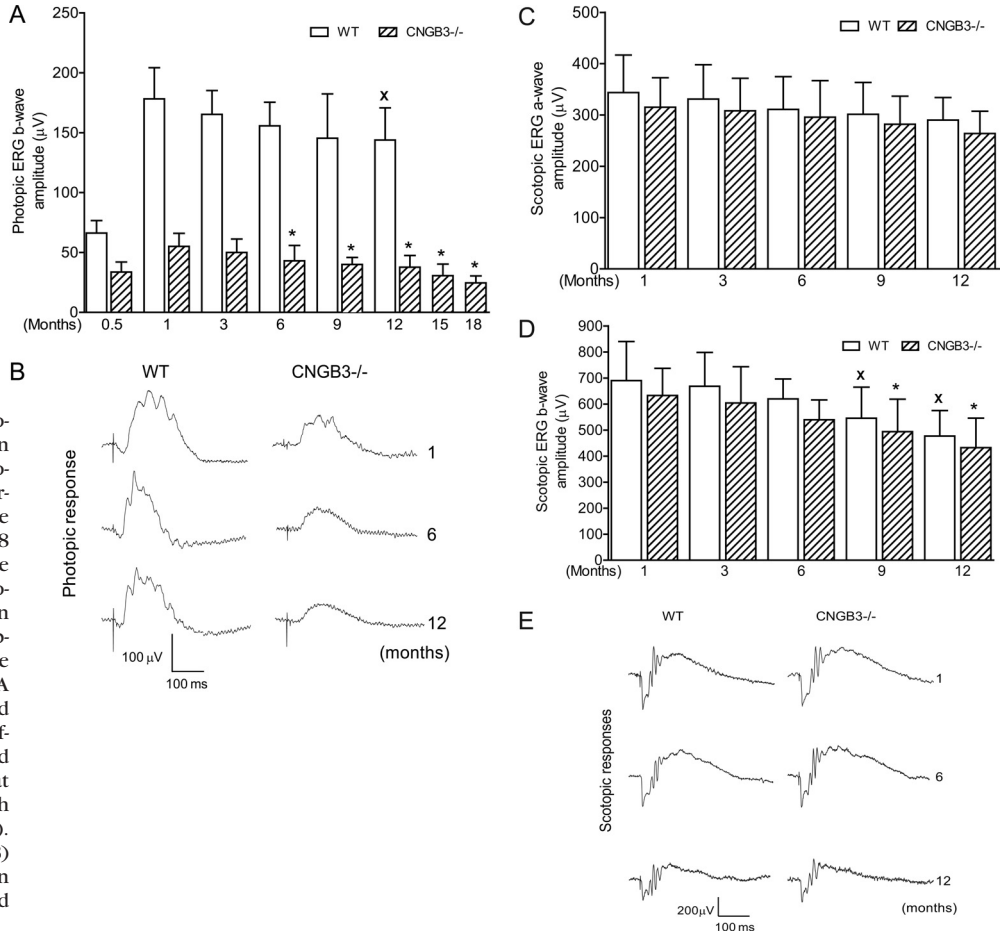

Figure 1. Early-onset, slow progression of cone dysfunction in CNGB3$^{-/-}$ mice. Photopic and scotopic ERG recordings were performed in CNGB3$^{-/-}$ and WT mice at various ages from P15 to 18 months. (**A**, **C**, **D**) Photopic b-wave (**A**), scotopic a-wave (**C**), and scotopic b-wave (**D**) amplitudes in CNGB3$^{-/-}$ and WT mice. Data represent mean ± SD (n = 5–12 mice for each group). One-way ANOVA (Newman-Keuls) analysis was used to determine significance among different ages ($^{*}P < 0.05$ compared with the value of CNGB3$^{-/-}$ mice at 1 month; $^{X}P < 0.05$ compared with the value of WT mice at 1 month). (**B**, **E**) Representative photopic (**B**) and scotopic (**E**) ERG traces in CNGB3$^{-/-}$ and WT mice at 1, 6, and 12 months.

significant difference in b-wave amplitude was observed in WT mice up to 12 months of age (Fig. 1A). Figure 1B shows representative traces of photopic ERG recordings in CNGB3$^{-/-}$ and WT mice at 1, 6, and 12 months. Hence, cone dysfunction in CNGB3$^{-/-}$ mice showed early onset and was slowly progressive.

We also evaluated rod function in CNGB3$^{-/-}$ mice at different ages by scotopic ERG recordings (Figs. 1C–E). Although there was a progressive reduction in the scotopic a- and b-waves of both WT and CNGB3$^{-/-}$ mice with age, there was no significant difference between the amplitudes of the a-waves or b-waves of age-matched CNGB3$^{-/-}$ and WT mice (Figs. 1C, 1D). Figure 1E shows representative traces of scotopic ERG recordings in CNGB3$^{-/-}$ and WT mice at 1, 6, and 12 months.

Early-Onset, Slow Progression of Cone Degeneration in CNGB3$^{-/-}$ Mice

We previously showed cone loss in CNGB3$^{-/-}$ mice at 1 month of age.[18] This included reduced cone density and increased photoreceptor apoptosis, as indicated by enhanced TUNEL labeling.[18] We extended those findings by examining the progression of cone loss in CNGB3$^{-/-}$ mice. Cone density in CNGB3$^{-/-}$ and WT mice at different ages was examined by cone opsin staining and PNA labeling of retinal whole mounts and retinal cross-sections. We found that although cone density starts to decrease as early as 1 month, cone degeneration in CNGB3$^{-/-}$ mice progresses only slowly. Figure 2 shows immunofluorescence labeling of S-opsin on the retinal whole mounts prepared from WT and CNGB3$^{-/-}$ mice at 1, 4, 8, and 12 months (Figs. 2Aa and 2Bb, respectively) and the corresponding quantification results (Fig. 2B; images of inferior quadrant shown. Labeling of other quadrants was similar; see Supplementary Fig. S1, http://www.iovs.org/lookup/suppl/doi:10.1167/iovs.10-6358/-/DCSupplemental). Cone density in CNGB3$^{-/-}$ mice at 1 month was approximately 80% of the WT level. This number was reduced to approximately 50% at 12 months. M-opsin staining and PNA labeling on the retinal whole mounts showed a similar pattern (see Supplementary Fig. S2, http://www.iovs.org/lookup/suppl/doi:10.1167/iovs.10-6358/-/DCSupplemental). The early-onset, slow progression of cone degeneration was also shown by labeling of cones in retinal cross-sections. Figure 3 shows M-opsin labeling on retinal sections prepared from WT (Fig. 3a) and CNGB3$^{-/-}$ (Fig. 3b) mice at P15 and at 1, 3, 6, and 12 months.

Cone degeneration in CNGB3$^{-/-}$ mice was also investigated by examining the expression of cone-specific proteins. Western blot analysis was performed to examine the expression of M-opsin, Gnat2, and CAR using retinal protein extracts prepared from CNGB3$^{-/-}$ and WT mice. As shown in Figure 4A, expression of these cone-specific proteins was significantly reduced in CNGB3$^{-/-}$ mice compared with WT mice, even at 1 month of age. Densitometric analysis showed that M-opsin, Gnat2, and CAR levels in CNGB3$^{-/-}$ retinas were significantly reduced at 1 month and were further reduced at 9 months compared with the age-matched WT mice (Fig. 4B). These results also are consistent with an early-onset, slow progression of cone degeneration in CNGB3$^{-/-}$ mice.

Cone degeneration in CNGA3$^{-/-}$ mice shows an asymmetric pattern, with cones in the inferior portion of the retina degenerating faster than in the superior retina.[29] We examined cone densities in the four different quadrants of retinal whole mounts prepared from CNGB3$^{-/-}$ mice to determine whether there was a topographic pattern of cone degeneration. Figure 5 shows M-opsin staining (Figs. 5Aa, WT; 5Ab, CNGB3$^{-/-}$) and PNA labeling (Figs. 5Ba, WT; 5Bb, CNGB3$^{-/-}$) on retinal whole

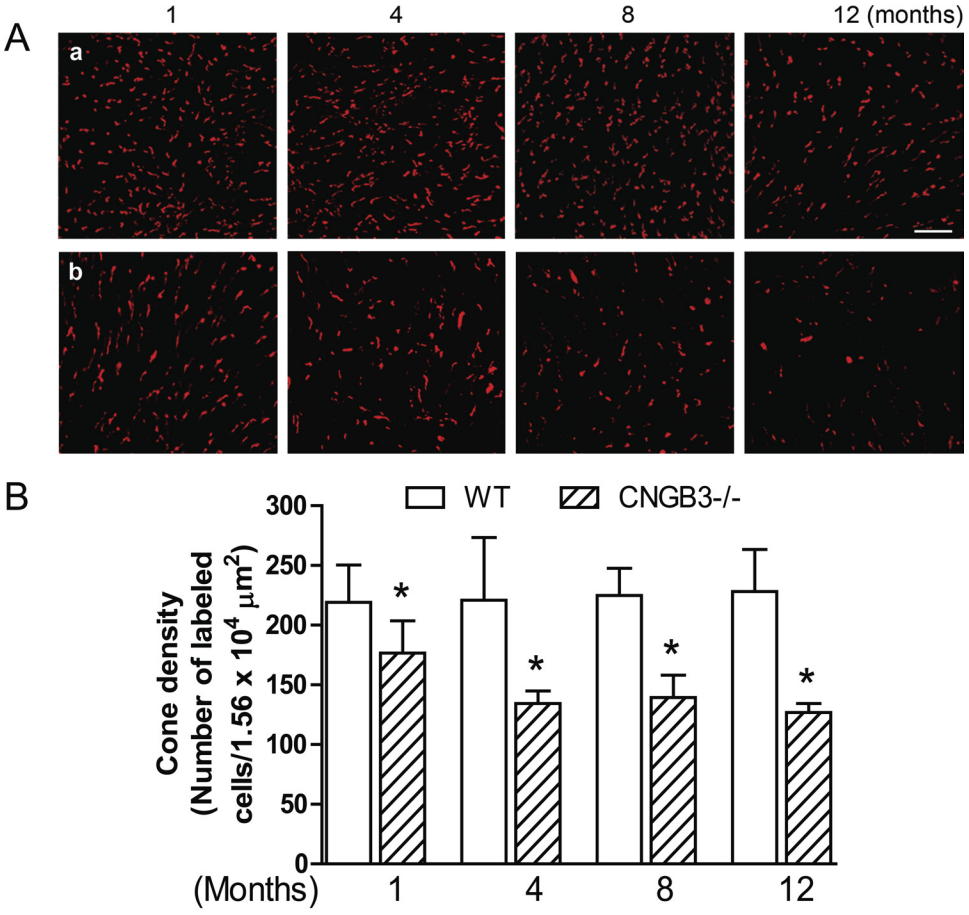

Figure 2. Early-onset, slow progression of cone degeneration in CNGB3$^{-/-}$ mice evaluated by immunofluorescence labeling of S-opsin on retinal whole mounts. Immunofluorescence labeling was performed on retinal whole mounts prepared from CNGB3$^{-/-}$ and WT mice at 1, 4, 8, and 12 months. (**A**) Representative confocal images of S-opsin labeling in the inferior quadrants of the retinal whole mounts prepared from WT (**a**) and CNGB3$^{-/-}$ (**b**) mice. Scale bar, 10 μm. (**B**) Quantitative analysis of S-opsin labeling in the inferior quadrants of the retinal whole mounts. Data represent mean ± SD (n = 4–9 mice for each group). Unpaired Student's t-test was used to determine significance between age-matched CNGB3$^{-/-}$ and WT mice (*P < 0.05).

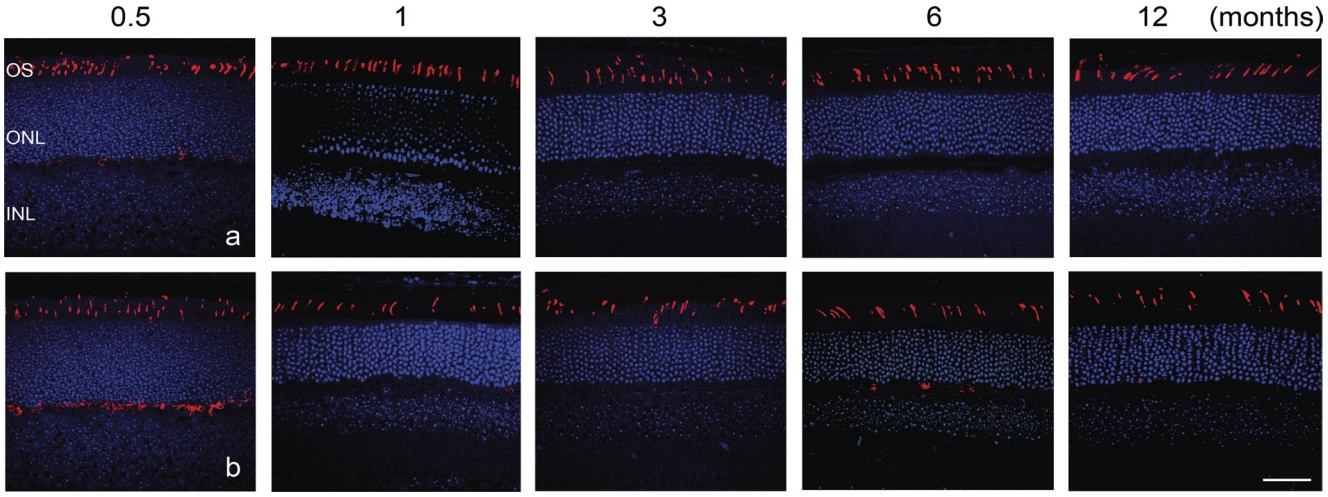

FIGURE 3. Early-onset, slow progression of cone degeneration in CNGB3$^{-/-}$ mice evaluated by immunofluorescence labeling of M-opsin on retinal cross-sections. Immunofluorescence labeling was performed on retinal cross-sections prepared from CNGB3$^{-/-}$ and WT mice at 0.5 (P15), 1, 3, 6, and 12 months. Shown are representative confocal images of M-opsin labeling on retinal cross-sections prepared from WT (**a**) and CNGB3$^{-/-}$ (**b**) mice. OS, outer segment; ONL, outer nuclear layer; INL, inner nuclear layer. Scale bar, 50 μm.

mounts prepared from CNGB3$^{-/-}$ and WT mice at 8 months and the corresponding quantitative analysis (Fig. 5C). Cone density in CNGB3$^{-/-}$ mice was approximately 72%, 70%, 78%, and 68% of the WT level for the superior, inferior, nasal, and temporal quadrants, respectively, as measured by M-opsin labeling (Fig. 5C, left), and was approximately 83%, 70%, 83%, and 78% of the WT level for the superior, inferior, nasal, and temporal quadrants, respectively, as measured by PNA labeling (Fig. 5C, right). Hence, the rate of cone degeneration in CNGB3$^{-/-}$ mice did not differ significantly among the four quadrants.

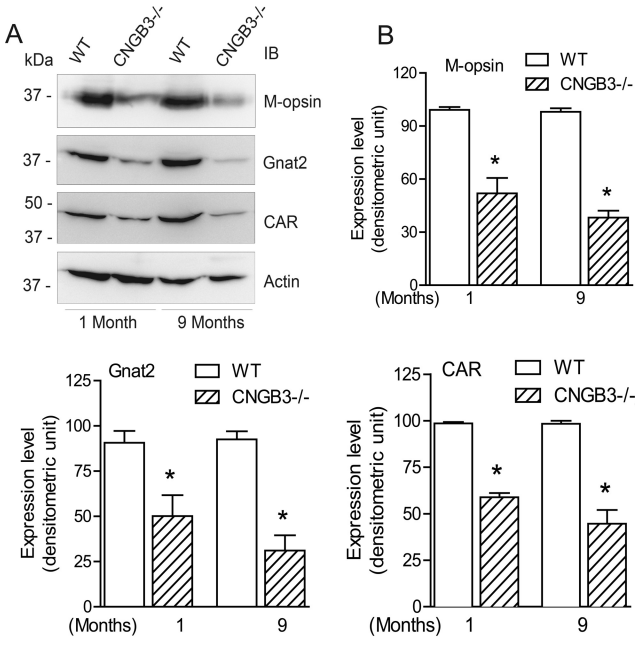

FIGURE 4. Early-onset, slow progression of cone degeneration in CNGB3$^{-/-}$ mice evaluated by Western blot detection of expression of cone-specific proteins. Western blot detection was performed using retinal membrane protein extracts prepared from CNGB3$^{-/-}$ and WT mice at 1 and 9 months to determine the expression of M-opsin, Gnat2, and CAR. Actin was included as a loading control. Shown are the representative images (**A**) of these blots and the corresponding quantification (**B**). Data represent mean ± SD (n = 4–7 mice for each group). Unpaired Student's t-test was used to determine significance between age-matched CNGB3$^{-/-}$ and WT mice (*$P < 0.05$).

Mislocalization of Cone Opsin

Disturbed trafficking of cone opsin was shown in CNGA3$^{-/-}$ mice.[29] We examined the localization of cone opsin in CNGB3$^{-/-}$ mice. Similar to reported results in CNGA3$^{-/-}$ mice,[29] we detected substantial amounts of opsin in the inner segments, ONL, and OPL of CNGB3$^{-/-}$ retina. This was particularly significant in young mice (P15). Figure 6A shows labeling for M-opsin and S-opsin on retinal cross-sections prepared from CNGB3$^{-/-}$ (Fig. 6Aa) and WT (Fig. 6Ab) mice at different ages. Figure 6B shows the quantitative results of the fluorescence intensity of M-opsin labeling in the OS, ONL, and OPL of the CNGB3$^{-/-}$ retina at P15 and P30, compared with that in the age-matched WT mice. Hence, CNGB3 deficiency, like CNGA3 deficiency, interferes with cone opsin trafficking to the outer segment.

Photoreceptor Terminals Are Unaffected by the Absence of CNGB3

To determine whether disruption of the synaptic terminals of the surviving cones might contribute to the decline in cone function noted in the ERG of the CNGB3$^{-/-}$ retina, we performed triple labeling of retinas from WT and CNGB3$^{-/-}$ mice for WGA, complexin III, and CtBP2 to visualize photoreceptor terminal distribution in the OPL, cone terminals, and synaptic ribbons, respectively (Fig. 7). The terminals of surviving cones and rods in the CNGB3$^{-/-}$ retina showed normal placement, continued to express appropriate synaptic proteins, and retained their synaptic ribbons. Similarly, surviving cone terminals also retained their flat synaptic contacts, as identified by PNA labeling (not shown). Rod and cone terminals showed normal terminal ultrastructure in the terminals of rods and cones (Fig. 8). Both rod and cone terminals in the WT and CNGB3$^{-/-}$ retina showed ribbon synaptic complexes with the triadic organization and ultrastructural features. As appropriate, cone terminals in the WT and CNGB3$^{-/-}$ retina had multiple ribbon complexes and formed flat contacts with OFF-cone bipolar cell dendrites. Together, these results suggest that decreased cone signals in the ERG arose primarily from dis-

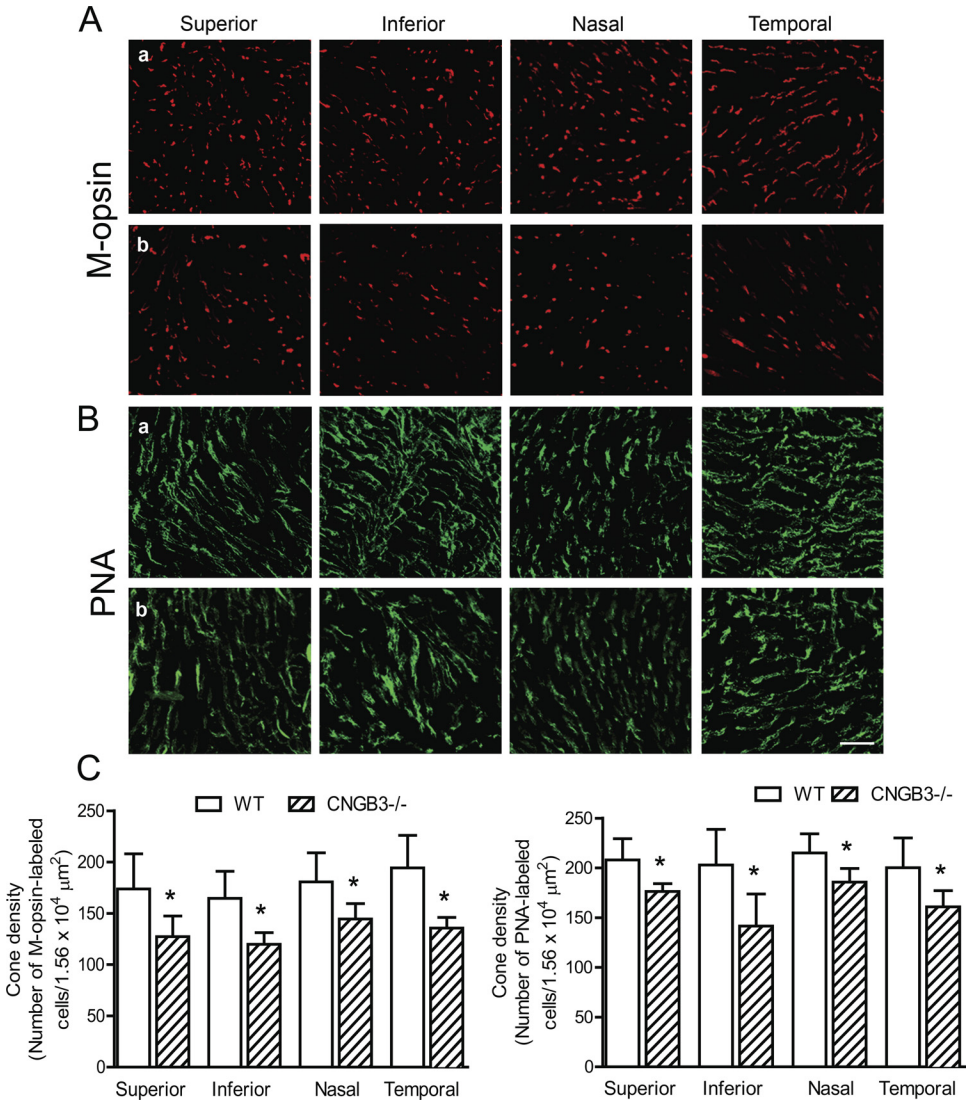

FIGURE 5. No topographic pattern of cone degeneration was found in CNGB3$^{-/-}$ mice. Immunofluorescence labeling for M-opsin and PNA staining was performed on retinal whole mounts prepared from CNGB3$^{-/-}$ and WT mice at 8 months. (**A**, **B**) Shown are confocal images of M-opsin labeling (**A**) and PNA labeling (**B**) on the quadrants of the retinal whole mounts prepared from WT (**a**) and CNGB3$^{-/-}$ mice (**b**). Scale bar, 10 μm. (**C**) Quantitative analysis of M-opsin labeling (*left*) and PNA labeling (*right*) on the quadrants of the retinal whole mounts. Data represent mean ± SD ($n = 4$ mice for each group). Unpaired Student's *t*-test was used to determine significance between age-matched CNGB3$^{-/-}$ and WT mice (*$P < 0.05$).

rupted cone phototransduction and cone degeneration rather than from synaptic disruption.

DISCUSSION

The high correlation of mutations in CNGB3 with human cone diseases implies a critical role for this protein in human cone function. We have previously shown impaired cone function and cone degeneration in CNGB3$^{-/-}$ mice[18] and provided the first experimental evidence supporting the link between mutations in CNGB3 and human cone diseases. This study demonstrates an early-onset (by P15, when the mouse eye opens), slow progression of cone dysfunction and degeneration arising from CNGB3 deficiency. The phenotype in CNGB3$^{-/-}$ mice is similar to the clinical symptoms of patients with CNGB3 mutations. It is important to note a phenotypic difference between human patients with achromatopsia, in whom there is an almost total lack of cone function from birth, and CNGB3$^{-/-}$ mice, in which some residual cone function persists as indicated by the ERG. The reason for this difference remains to be identified but may be related to the heterogenetic causes of achromatopsia (three other genes have been identified in achromatopsia patients in addition to CNGB3) and species differences. A more thorough clinical phenotype/genetic disorder relationship study may help to better address this question. It is also worth noting that the residual cone function in CNGB3$^{-/-}$ mice was not comparable to the percentage of cones that remained. The cone ERG response at 1 month was only approximately 30% of the WT level, whereas approximately 80% of cones remained at this age. Similarly, the cone response at 12 months was only approximately 20% of the WT level, whereas more than 50% of cones remained at this age in the CNG3B$^{-/-}$ retina. In contrast, the reduction of cone response (approximately 70%–80%) did approximate the reduction of cone proteins (i.e., M-opsin, Gnat2, and CAR, which were reduced by approximately 50%–70%; see Fig. 4). Thus, although ample cones remained in the CNGB3-deficient retina as late as 12 months of age, the functional response and expression of phototransduction proteins of the surviving cones were seriously impaired. Indeed, we cannot exclude the possibility that an altered protein expression in cones also could contribute to the functional deficits. Furthermore, our studies showed that the terminals of cones and rods in the CNGB3$^{-/-}$ retina had normal placement in the OPL and retained their appropriate synaptic components and ultrastructural organization. These findings suggest that the cone-signaling deficits observed arose from phototransduction deficits and progressive cone loss rather than from synaptic defects. Consistent with this finding, most of the surviving cones in the CNGA3$^{-/-}$ retina have morphologically normal synapses,[29]

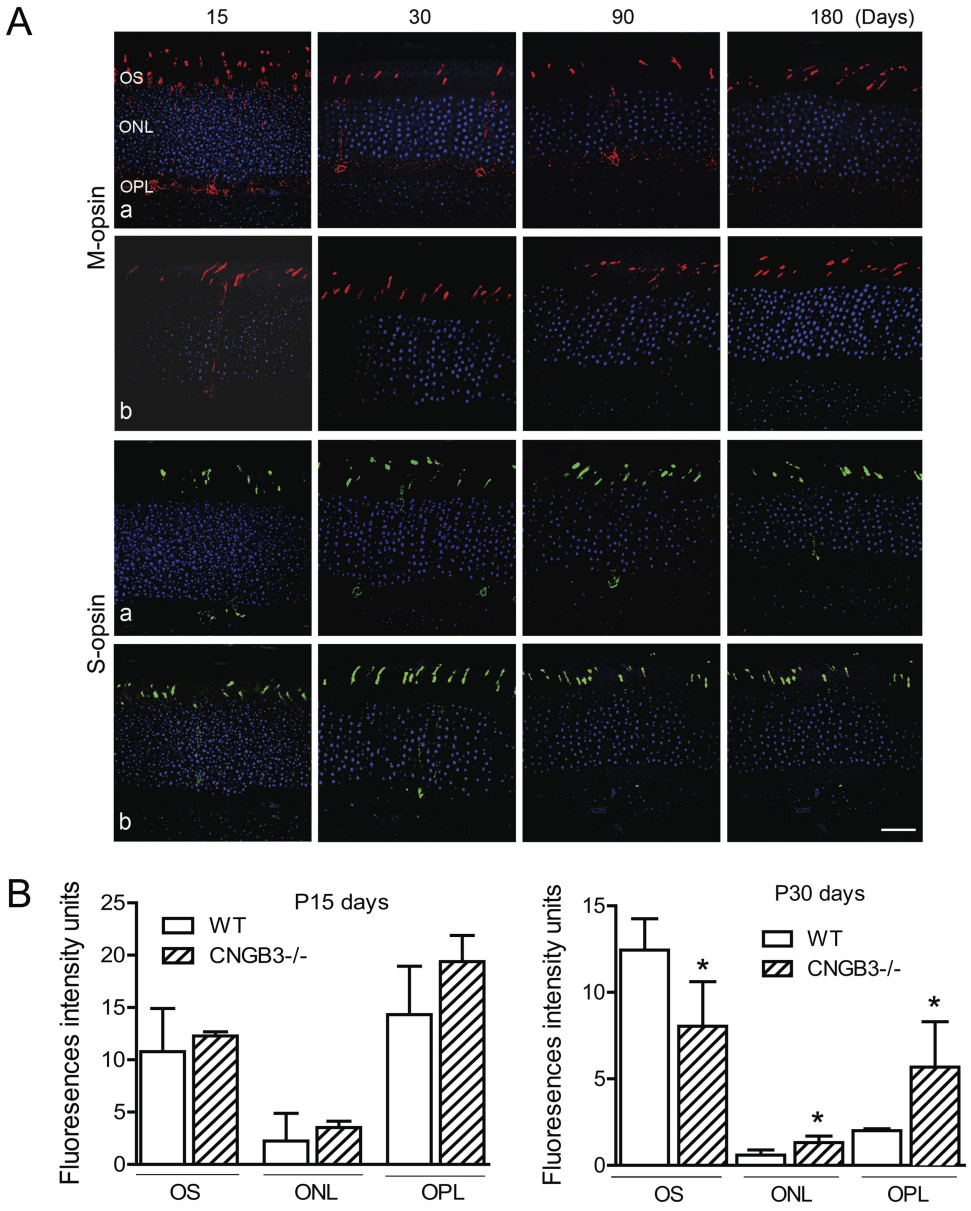

FIGURE 6. Mislocalization of cone opsin in CNGB3$^{-/-}$ mice. Immunofluorescence labeling of cone opsin was performed on retinal cross-sections prepared from CNGB3$^{-/-}$ and WT mice at P15, P30, P90, and P180. (**A**) Shown are the representative confocal images of M-opsin and S-opsin labeling on the retinal sections prepared from CNGB3$^{-/-}$ (**a**) and WT (**b**) mice. OS, outer segment; ONL, outer nuclear layer; OPL, outer plexiform layer. Scale bar, 100 μm. (**B**) Quantitative analysis of the fluorescence intensities of M-opsin labeling in the OS, ONL, and OPL regions. Data represent mean ± SD (n = 4 mice for each group). Unpaired Student's t-test was used to determine significance ($^*P < 0.05$).

and mice lacking both functional cones and rods (CNGA3$^{-/-}$/Rho$^{-/-}$) have structurally normal synaptic contacts until the time of complete loss of photoreceptors.[30]

Cone degeneration has been shown in a variety of mouse lines that are deficient in cone-specific or cone-dominant proteins, such as cpfl1 (with cone PDE6C deficiency),[31] RetGC1$^{-/-}$,[32–34] and GCAP$^{-/-}$ (and GCAP L151F, Y99C mutant) mice.[35] Mutations in these genes in humans are associated with cone defects[36,3738] However, the retinal pathogenesis and disease progression in these mouse lines differ substantially from one another. Cone degeneration in cpfl1 mice has an early-onset, rapid progression; by 2 to 3 months, most of the cones (90%) are lost.[31] In contrast, cone degeneration in RetGC1$^{-/-}$ mice has a relatively late onset, with normal numbers of cone cells at 4 and 5 weeks of age and then gradually decreasing by 6 months.[34] This work and the study by Michalakis et al.[29] showed that cone degeneration in CNG channel deficiency is of early-onset, slow progression. Of note, there is no clear cone degeneration in the mouse line with Gnat2 deficiency,[39] although cone transduction is completely blocked in these mice. Thus, although deficiency of these molecules—which are involved directly or indirectly in the phototransduction cascade—leads to a common consequence (i.e., blockade or impairment of cone phototransduction), the progression of cone degeneration varies. The underlying mechanisms, therefore, might be expected to be distinct. It is also worth noting that even with deficiencies of the same gene, phenotypes can vary among species. A slow progression of cone degeneration with late onset is observed in canines with CNGB3 mutation or CNGB3 deficiency. In contrast to what we have found in the present study in mice, cone density does not start to decrease in CNGB3-deficient dogs until nearly 2 years of age (G. Aguirre, University of Pennsylvania, personal communication).

Little is known about the mechanism of cone degeneration in CNG channel deficiency. Cone degeneration in CNGB3$^{-/-}$ and CNGA3$^{-/-}$ mice is likely attributable to a decrease or loss of the functional channels and subsequent impairment or loss of cone phototransduction. We[18] and others[29] have shown that cone death occurs in CNG channel deficiency primarily by way of an apoptotic mechanism, but the molecular pathway connecting CNG channel deficiency to cone apoptotic death

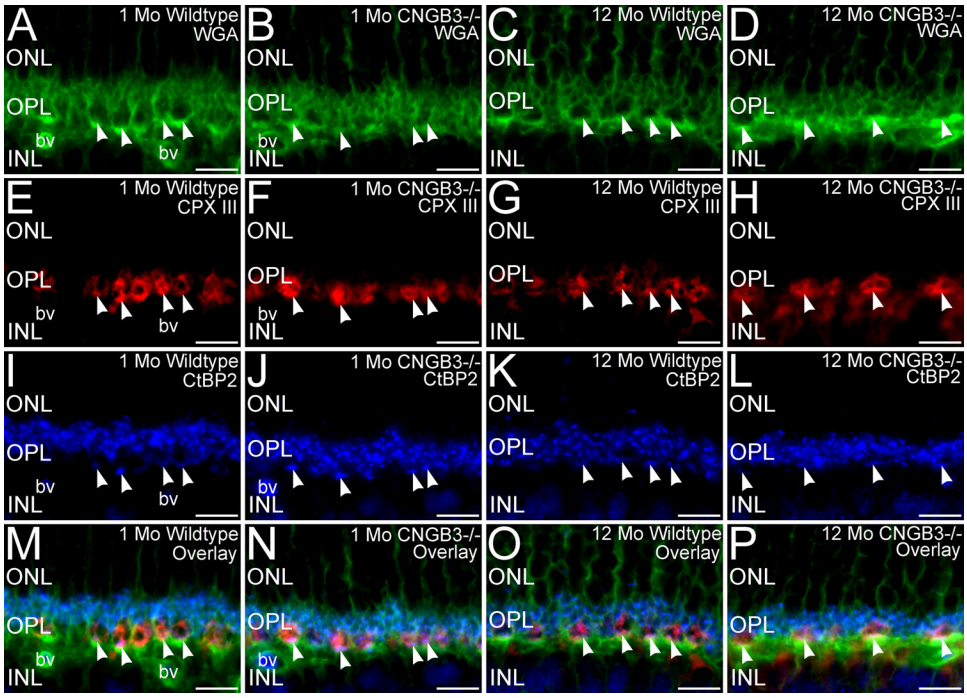

FIGURE 7. Surviving cone terminals in the CNGB3$^{-/-}$ retina show normal characteristics. Retinas from WT and CNGB3$^{-/-}$ mice at 1 and 12 months of age triple labeled for WGA (*green*, **A–D**), complexin III (CPX III, *red*, **E–H**), and CtBP2 (*blue*, **I–L**) to visualize photoreceptor terminal distribution, cone terminals, and synaptic ribbons, respectively. The absence of CNGB3 does not disrupt OPL organization, cone terminals (*arrowheads*), or the synaptic ribbons in rod and cone terminals. WT mouse retina at 1 (**A**, **E**, **I**, **M**) and 12 months of age (**C**, **G**, **K**, **O**). CNGB3$^{-/-}$ mouse retina at 1 (**B**, **F**, **J**, **N**) and 12 (**D**, **H**, **L**, **P**) months of age. ONL, outer nuclear layer; OPL, outer plexiform layer; INL, inner nuclear layer; bv, blood vessel. Scale bars, 10 μm.

remains to be elucidated. It is recognized that studying the mechanism of cone degeneration in a rod-dominant mammalian retina is challenging because cones account for only 3% to 5% the photoreceptor population. We have recently shown that the cone-dominant Nrl$^{-/-}$ mouse line (deficiency of *n*eural *r*etinal *l*eucine zipper transcription factor) is a valuable model for the study of cone CNG channel function and structure.[17] The Nrl$^{-/-}$ retina expresses abundant cone CNG channels and lacks expression of the rod CNG channel.[17] Hence, the mouse lines with CNG channel deficiency in a cone-dominant retina (i.e., CNGA3$^{-/-}$/Nrl$^{-/-}$ and CNGB3$^{-/-}$/Nrl$^{-/-}$ mice) could be valuable models in which to study the mechanism of cone degeneration. One way to explore the triggering factors involved in cone degeneration is to examine the direct/immediate cellular consequences of CNGB3 deficiency. One strong possibility is that the cellular consequences of CNG channel deficiency (i.e., a lowered intracellular Ca^{2+} concentration and the subsequent accumulation of cGMP) may trigger cone death. Indeed, we observed a dramatically increased level of cGMP in CNGA3$^{-/-}$/Nrl$^{-/-}$ mice at a young age (P10-P30 days) that correlated with cone apoptosis (our unpublished observation). This observation suggests a potential role for cGMP accumulation in the early-onset cone degeneration in CNG channel deficiency. Cone degeneration in CNGB3$^{-/-}$ mice might also be associated with a role of CNGB3 in outer segment morphogenesis and integrity, similar to its rod counterpart CNGB1, which is known to play a role in rod outer segment disc morphogenesis.[40] Our work showing outer segment disorganization[18] in some cones of CNGB3$^{-/-}$ mice is consistent with this finding. The early onset of cone degeneration in CNG channel deficiency may be related to the mislocalization of cone opsin. Mislocalization of cone opsin in CNGB3$^{-/-}$ mice (this study) and CNGA3$^{-/-}$ mice[29] was more profound in developing and young animals and correlated with cone apoptosis at the same age. Mislocalization of cone opsin is a strong candidate to induce cellular stress and apoptosis.[41] It would be of great clinical significance to identify the factors that contribute to the early-onset degeneration. The double knockout CNGA3$^{-/-}$/Nrl$^{-/-}$ and CNGB3$^{-/-}$/Nrl$^{-/-}$ mouse lines could be useful models for these studies. One potentially useful application of these models would be to identify gene/protein expression profiles using microarray/proteomic analyses with retinal preparations from young and old mice compared with age-matched Nrl$^{-/-}$ controls.

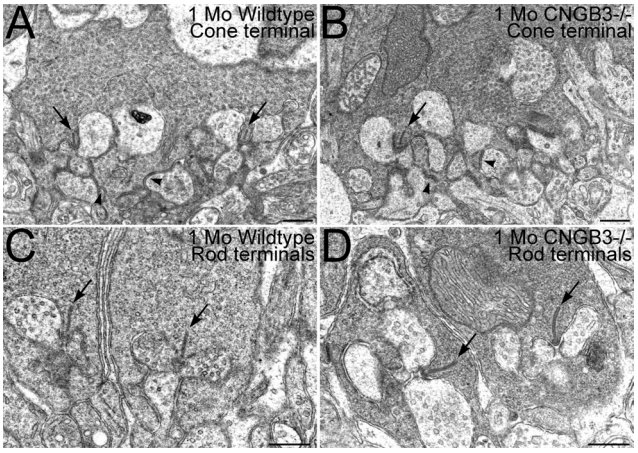

FIGURE 8. Ultrastructural organization of rod and cone synapses is normal in the CNGB3$^{-/-}$ retina. Cone terminals in the WT (**A**) and CNGB3$^{-/-}$ (**B**) retina showed ribbon synaptic complexes organized around a synaptic ribbon (*arrows*) and abundant synaptic vesicles presynaptically, with the normal postsynaptic triad of horizontal cell processes flanking the ribbon laterally and ON-cone bipolar cell dendrites occupying a position beneath the ribbon. Flat contacts with OFF-cone bipolar cell dendrites also were present (*arrowheads*). Rod terminals in the WT (**C**) and CNGB3$^{-/-}$ (**D**) retina also showed normal synaptic ultrastructure and ribbon synaptic complexes. All terminals are from specimens at 1 month of age. Scale bar, 0.5 μm.

Mislocalization of cone opsin is observed in both CNGA3$^{-/-}$ and CNGB3$^{-/-}$ mice, suggesting that it is the functional channel complex, rather than the individual subunit, that is critical for the normal trafficking and outer segment targeting of cone opsin. The molecular details of cone opsin trafficking, however, are not yet known. In rod photoreceptors, rhodopsin is synthesized in the inner segment and

then is actively transported through the connecting cilium into the outer segment.[42,43] An equivalent mechanism may exist in cones and could be impaired in CNG channel deficiency. Nevertheless, although the channel-deficient cones are able to synthesize opsins, they failed to transport or retain the protein properly into the outer segments. Mislocalization of cone opsin could have two potential consequences. First, it might be associated (or partially associated) with cellular stress and apoptosis.[41] Second, the mislocalized opsin might be degraded more easily than the normal localized opsin. Indeed, the expression level of M-opsin in the CNGB3$^{-/-}$ retina is significantly reduced (see Fig. 4). We have shown previously that the mRNA level for cone opsin in CNGB3$^{-/-}$ mice is comparable to that of WT mice,[18] suggesting that the reduction in the opsin protein level is likely due to enhanced degradation rather than decreased synthesis.

In summary, this work provides experimental evidence showing the nature of early-onset, slow progression of cone dysfunction and degeneration in CNGB3 deficiency. The phenotype of CNGB3$^{-/-}$ mice is similar in many respects to the symptoms in human patients with mutations of CNGB3. Thus, the CNGB3-deficient mouse line could serve as a valuable model in which to study the retinal pathogenesis of CNG channel deficiency and the mechanism of cone degeneration.

Acknowledgments

The authors thank Cynthia Harry and Barbara Nagel for providing excellent technical assistance.

References

1. Hirano AA, Hack I, Wassle H, Duvoisin RM. Cloning and immunocytochemical localization of a cyclic nucleotide-gated channel alpha-subunit to all cone photoreceptors in the mouse retina. *J Comp Neurol.* 2000;421:80–94.
2. Zagotta WN, Siegelbaum SA. Structure and function of cyclic nucleotide-gated channels. *Annu Rev Neurosci.* 1996;19:235–263.
3. Kaupp UB, Seifert R. Cyclic nucleotide-gated ion channels. *Physiol Rev.* 2002;82:769–824.
4. Pugh EN Jr, Lamb TD. *Handbook of Biological Physics*. Amsterdam: Elsevier/North-Holland; 2000:183.
5. Rebrik TI, Korenbrot JI. In intact cone photoreceptors, a Ca^{2+}-dependent, diffusible factor modulates the cGMP-gated ion channels differently than in rods. *J Gen Physiol.* 1998;112:537–548.
6. Gerstner A, Zong X, Hofmann F, Biel M. Molecular cloning and functional characterization of a new modulatory cyclic nucleotide-gated channel subunit from mouse retina. *J Neurosci.* 2000;20:1324–1332.
7. Dryja TP, Finn JT, Peng YW, McGee TL, Berson EL, Yau KW. Mutations in the gene encoding the alpha subunit of the rod cGMP-gated channel in autosomal recessive retinitis pigmentosa. *Proc Natl Acad Sci U S A.* 1995;92:10177–10181.
8. Kohl S, Baumann B, Broghammer M, et al. Mutations in the CNGB3 gene encoding the beta-subunit of the cone photoreceptor cGMP-gated channel are responsible for achromatopsia (ACHM3) linked to chromosome 8q21. *Hum Mol Genet.* 2000;9:2107–2116.
9. Kohl S, Varsanyi B, Antunes GA, et al. CNGB3 mutations account for 50% of all cases with autosomal recessive achromatopsia. *Eur J Hum Genet.* 2005;13:302–308.
10. Nishiguchi KM, Sandberg MA, Gorji N, Berson EL, Dryja TP. Cone cGMP-gated channel mutations and clinical findings in patients with achromatopsia, macular degeneration, and other hereditary cone diseases. *Hum Mutat.* 2005;25:248–258.
11. Wissinger B, Gamer D, Jagle H, et al. CNGA3 mutations in hereditary cone photoreceptor disorders. *Am J Hum Genet.* 2001;69:722–737.
12. Kohl S, Baumann B, Rosenberg T, et al. Mutations in the cone photoreceptor G-protein alpha-subunit gene GNAT2 in patients with achromatopsia. *Am J Hum Genet.* 2002;71:422–425.
13. Johnson S, Michaelides M, Aligianis IA, et al. Achromatopsia caused by novel mutations in both CNGA3 and CNGB3. *J Med Genet.* 2004;41:e20.
14. Wiszniewski W, Lewis RA, Lupski JR. Achromatopsia: the CNGB3 p.T383fsX mutation results from a founder effect and is responsible for the visual phenotype in the original report of uniparental disomy 14. *Hum Genet.* 2007;121:433–439.
15. Faillace MP, Bernabeu RO, Korenbrot JI. Cellular processing of cone photoreceptor cyclic GMP-gated ion channels: a role for the S4 structural motif. *J Biol Chem.* 2004;279:22643–22653.
16. Peng C, Rich ED, Varnum MD. Achromatopsia-associated mutation in the human cone photoreceptor cyclic nucleotide-gated channel CNGB3 subunit alters the ligand sensitivity and pore properties of heteromeric channels. *J Biol Chem.* 2003;278:34533–34540.
17. Matveev AV, Quiambao AB, Browning Fitzgerald J, Ding XQ. Native cone photoreceptor cyclic nucleotide-gated channel is a heterotetrameric complex comprising both CNGA3 and CNGB3: a study using the cone-dominant retina of Nrl$^{-/-}$ mice. *J Neurochem.* 2008;106:2042–2055.
18. Ding XQ, Harry CS, Umino Y, Matveev AV, Fliesler SJ, Barlow RB. Impaired cone function and cone degeneration resulting from CNGB3 deficiency: down-regulation of CNGA3 biosynthesis as a potential mechanism. *Hum Mol Genet.* 2009;18:4770–4780.
19. Ding XQ, Nour M, Ritter LM, Goldberg AF, Fliesler SJ, Naash MI. The R172W mutation in peripherin/rds causes a cone-rod dystrophy in transgenic mice. *Hum Mol Genet.* 2004;13:2075–2087.
20. Chakraborty D, Ding XQ, Conley SM, Fliesler SJ, Naash MI. Differential requirements for retinal degeneration slow intermolecular disulfide-linked oligomerization in rods versus cones. *Hum Mol Genet.* 2009;18:797–808.
21. Ding XQ, Fitzgerald JB, Matveev AV, McClellan ME, Elliott MH. Functional activity of photoreceptor cyclic nucleotide-gated channels is dependent on the integrity of cholesterol- and sphingolipid-enriched membrane domains. *Biochemistry.* 2008;47:3677–3687.
22. Matveev AV, Fitzgerald JB, Xu J, Malykhina AP, Rodgers KK, Ding XQ. The disease-causing mutations in the carboxyl terminus of the cone cyclic nucleotide-gated channel CNGA3 subunit alter the local secondary structure and interfere with the channel active conformational change. *Biochemistry.* 2010;49:1628–1639.
23. Komeima K, Rogers BS, Lu L, Campochiaro PA. Antioxidants reduce cone cell death in a model of retinitis pigmentosa. *Proc Natl Acad Sci U S A.* 2006;103:11300–11305.
24. Sherry DM, Murray AR, Kanan Y, et al. Lack of protein-tyrosine sulfation disrupts photoreceptor outer segment morphogenesis, retinal function and retinal anatomy. *Eur J Neurosci* 32:1461–1472.
25. Farjo R, Skaggs JS, Nagel BA, et al. Retention of function without normal disc morphogenesis occurs in cone but not rod photoreceptors. *J Cell Biol.* 2006;173:59–68.
26. Mears AJ, Kondo M, Swain PK, et al. Nrl is required for rod photoreceptor development. *Nat Genet.* 2001;29:447–452.
27. Peachey NS, Goto Y, al-Ubaidi MR, Naash MI. Properties of the mouse cone-mediated electroretinogram during light adaptation. *Neurosci Lett.* 1993;162:9–11.
28. Raz-Prag D, Ayyagari R, Fariss RN, et al. Haploinsufficiency is not the key mechanism of pathogenesis in a heterozygous Elovl4 knockout mouse model of STGD3 disease. *Invest Ophthalmol Vis Sci.* 2006;47:3603–3611.
29. Michalakis S, Geiger H, Haverkamp S, Hofmann F, Gerstner A, Biel M. Impaired opsin targeting and cone photoreceptor migration in the retina of mice lacking the cyclic nucleotide-gated channel CNGA3. *Invest Ophthalmol Vis Sci.* 2005;46:1516–1524.
30. Claes E, Seeliger M, Michalakis S, Biel M, Humphries P, Haverkamp S. Morphological characterization of the retina of the CNGA3(−/−)Rho(−/−) mutant mouse lacking functional cones and rods. *Invest Ophthalmol Vis Sci.* 2004;45:2039–2048.
31. Fischer MD, Tanimoto N, Beck SC, et al. Structural and functional phenotyping in the cone-specific photoreceptor function loss 1 (cpfl1) mouse mutant: a model of cone dystrophies. *Adv Exp Med Biol.* 664:593–599.
32. Baehr W, Karan S, Maeda T, et al. The function of guanylate cyclase 1 and guanylate cyclase 2 in rod and cone photoreceptors. *J Biol Chem.* 2007;282:8837–8847.

33. Yang RB, Robinson SW, Xiong WH, Yau KW, Birch DG, Garbers DL. Disruption of a retinal guanylyl cyclase gene leads to cone-specific dystrophy and paradoxical rod behavior. *J Neurosci.* 1999; 19:5889–5897.
34. Coleman JE, Zhang Y, Brown GA, Semple-Rowland SL. Cone cell survival and downregulation of GCAP1 protein in the retinas of GC1 knockout mice. *Invest Ophthalmol Vis Sci.* 2004;45:3397–3403.
35. Mendez A, Chen J. Mouse models to study GCAP functions in intact photoreceptors. *Adv Exp Med Biol.* 2002;514:361–388.
36. Kelsell RE, Gregory-Evans K, Payne AM, et al. Mutations in the retinal guanylate cyclase (RETGC-1) gene in dominant cone-rod dystrophy. *Hum Mol Genet.* 1998;7:1179–1184.
37. Olshevskaya EV, Ermilov AN, Dizhoor AM. Factors that affect regulation of cGMP synthesis in vertebrate photoreceptors and their genetic link to human retinal degeneration. *Mol Cell Biochem.* 2002;230:139–147.
38. Newbold RJ, Deery EC, Payne AM, Wilkie SE, Hunt DM, Warren MJ. Guanylate cyclase activating proteins, guanylate cyclase and disease. *Adv Exp Med Biol.* 2002;514:411–438.
39. Chang B, Dacey MS, Hawes NL, et al. Cone photoreceptor function loss-3, a novel mouse model of achromatopsia due to a mutation in Gnat2. *Invest Ophthalmol Vis Sci.* 2006;47:5017–5021.
40. Zhang Y, Molday LL, Molday RS, et al. Knockout of GARPs and the beta-subunit of the rod cGMP-gated channel disrupts disk morphogenesis and rod outer segment structural integrity. *J Cell Sci.* 2009;122:1192–1200.
41. Taylor J, Hardy J, Fischbeck K. Toxic proteins in neurodegenerative disease. *Science.* 2002;296:1991–1995.
42. Liu X, Udovichenko I, Brown S, Steel K, Williams D. Myosin VIIa participates in opsin transport through the photoreceptor cilium. *J Neurosci.* 1999;19:6267–6274.
43. Williams D. Transport to the photoreceptor outer segment by myosin VIIa and kinesin II. *Vision Res 2002.* 2002;42:455–462.